



Wayne State University

Civil and Environmental Engineering Faculty
Research Publications

Civil and Environmental Engineering

10-24-2016

Collapse Resistance of Moment Resisting Frame and Shear Wall RC Structural Systems Exposed to Blast

Alaa I. Chehab

Wayne State University, alaa.chehab@wayne.edu

Christopher D. Eamon

Wayne State University, eamon@eng.wayne.edu

Joshua Griffin

Kimley-Horn, josh.griffin@kimley-horn.com

Recommended Citation

Chehab Alaa, I., Eamon Christopher, D., & Griffin, J. (2017). Collapse Resistance of RC Moment-Resisting Frame and Shear Wall Structural Systems Exposed to Blast. *Journal of Performance of Constructed Facilities*, 31(2), 04016099.

doi:10.1061/(ASCE)CF.1943-5509.0000957

Available at: https://digitalcommons.wayne.edu/ce_eng_frp/25

This Article is brought to you for free and open access by the Civil and Environmental Engineering at DigitalCommons@WayneState. It has been accepted for inclusion in Civil and Environmental Engineering Faculty Research Publications by an authorized administrator of DigitalCommons@WayneState.

1 **Collapse Resistance of Moment Resisting Frame and Shear Wall RC Structural Systems**
2 **Exposed to Blast**

Alaa I. Chehab, A.M.ASCE¹; Christopher D. Eamon, M.ASCE²; and Joshua Griffin³

3
4 **Abstract**

5 Various characteristics of a structure influence its response when subjected to a blast load. This
6 has important implications for survivability and resistance to progressive collapse. In this study,
7 the effect of the type of lateral load resisting system on reinforced concrete building resistance to
8 progressive collapse when exposed to blast load is examined. Fourteen different reinforced
9 concrete structures were considered for analysis, with five structures designed as moment
10 resisting frames and nine designed as shear walls systems. Buildings with 3, 6, and 10 stories
11 with 3, 4, and 5-bay symmetric configurations were considered. The structures were exposed to
12 external and internal charges, while the nonlinear, transient dynamic analysis of collapse
13 behavior was investigated with a finite element based approach, the applied element method
14 (AEM). The results show that the shear wall structures and structures larger in height and plan
15 generally provide greatest resistance to blast damage and progressive collapse.

16
17 **Keywords:** RC structures; Progressive collapse; FEM; AEM; Shear walls; Blast Loads.

18

¹ Ph.D. Candidate, Dept. of Civil and Environmental Engineering, Wayne State University, Detroit, MI 48202.
E-mail: alaa.chehab@wayne.edu

² Associate Professor, Dept. of Civil and Environmental Engineering, Wayne State University. E-mail:
eamon@eng.wayne.edu

³ Structural Engineer, Kimley-Horn, Raleigh, NC 27601. E-mail: josh.griffin@kimley-horn.com

19 **Introduction**

20 Progressive collapse refers to the phenomenon where failure of a structural component
21 causes or contributes to the collapse of adjoining members, which then causes additional collapse
22 of the structure (GSA 2003). Since the events of 9-11, various research studies have been
23 undertaken to further examine extreme load events and to suggest how corresponding damage
24 may be mitigated. From these efforts, several analyses and design guidelines to improve
25 structure resistance to progressive collapse have been developed (ASCE 2010; GSA 2003;
26 USDOD 2005). Of the research work available, some focused specifically on modeling the
27 World Trade Center events (Bazant and Zhou 2002; Wierzbicki and Teng 2003; Lynn and Isobe
28 2007), while others evaluated the effectiveness of different blast modeling approaches in general
29 (Powell 2005; Li and Shi 2008). Approaching this issue from a probabilistic perspective and
30 considering the interaction of other extreme loads, Asprone et al. (2010) proposed a probabilistic
31 model for multi-hazard risk associated with the limit state of collapse for a generic four story
32 reinforced concrete structure, subjected to blast in the presence of seismic risk. Later, Málaga-
33 Chuquitaype et al. (2016) investigated the influence of secondary frames on the mitigation of
34 collapse in steel structures subjected to earthquake and blast scenarios, as well as localized fire
35 and blast hazards.

36 A larger number of research efforts studied idealized buildings of steel or reinforced
37 concrete from a deterministic approach. Among the existing studies of steel moment frame
38 structures, Grierson et al. (2005), Zhang et al. (2010) and later Korol et al. (2011), presented a
39 progressive collapse analysis, while Hamburger and Whittaker (2004) found that frames might
40 resist collapse by redistributing loads to adjacent columns. The performance of steel braced
41 frames that were subjected to sudden removal of a first story column was investigated by Kim et

42 al. (2008), while a similar analysis was presented by Gross and McGuire (1983). Alashker and
43 El-Tawil (2011) discussed the use of calibrated macro-models to model progressive collapse, and
44 a design-oriented model was proposed for computing the load resisting capacity of composite
45 steel-concrete floors subjected to interior column loss. They concluded that the macro and micro
46 models produced similar collapse response.

47 Various studies considered the analysis of reinforced concrete structures as well.
48 Nonlinear pushover analyses (nonlinear static procedure) of reinforced concrete walls coupled by
49 steel beams have been discussed (El-Tawil et al. 2002). Several investigated the behavior of the
50 structure when exposed to an explosion near ground level (Almusallam et al. 2010; Xu and Liu
51 2009), while Sasani et al. (2011) used experimental data and analytical results to evaluate the
52 progressive collapse resistance of an actual building that followed severe initial damage. Rather
53 than simulate an explosion, others simply instantaneously removed ground floor columns to
54 study the potential effect of severe damage (Sasani and Sagiroglu 2008; Hong et al. 2006).

55 The studies above provide a relatively small but significant body of knowledge regarding
56 progressive collapse under extreme blast load events. Although both steel and reinforced
57 concrete structures were considered, the existing research has been limited to moment resisting
58 and braced frame buildings, whereas structures that use shear walls for lateral load resistance
59 have not been considered in detail. However, this type of system may in fact display a
60 significantly different performance when exposed to blast loads than frame-type buildings. For
61 example, on January 25, 1971, while under construction, the floor slabs of the 16 story 2000
62 Commonwealth Avenue building in Boston, MA failed, resulting in a progressive collapse of
63 approximately 60% of the building. However, the progressive failure stopped at the location of
64 the shear walls surrounding the elevator core, saving the remaining portion of the building

65 (Granger et al. 1971). This type of behavior is generally not seen with similar moment frame
66 and braced frame buildings. However, the typical differences in behavior for these structures
67 exposed to blast loads are currently not well quantified. Thus, the objective of this study is to
68 investigate the difference in progressive collapse performance between a selection of reinforced
69 concrete structures with shear walls systems and corresponding structures with moment resisting
70 frames when exposed to blast loads.

71 **Structures Considered**

72 Two sets of hypothetical structures were designed according to American Concrete
73 Institute (ACI) 318-11 Code Standards, where one set was designed to resist the lateral loads
74 using a moment resisting frame (MRF), and the other using a shear wall system. The buildings
75 were assumed to be located in Detroit, Michigan, and design loads were determined according to
76 ASCE 7-10 for office building occupancy, resulting in a dead to live load ratio of approximately
77 1.5:1. As load combinations involving seismic loads were found not to govern, wind loads were
78 used for lateral design and were determined with the directional procedure. As no special
79 seismic detailing was required, the structures were designed as ordinary moment frames and
80 shear walls that satisfied general ACI 318 reinforcing requirements for continuity and structural
81 integrity. Three building geometries were considered for analysis; symmetric 10 story structures
82 with either 3x3, 4x4, or 5x5 bays, where all columns are spaced at 6.1 m. Additional 4x4
83 structures of 3 and 6 stories were also designed to examine the effect of building height, as
84 discussed below. In all structures, the first floor height is taken as 4.3 m and the remaining floor
85 heights are 3.7 m, with slab thickness of 180-200 mm. Slab reinforcement is taken as #5 (15.8
86 mm) bars with 25.4 mm cover. Columns are 355 (3 story buildings), 460 (6 story buildings), and
87 560 mm (10 story buildings) square and are taken to have fixed supports on the ground floor. As

88 necessary to meet code strength requirements, total column longitudinal reinforcement area
89 varied, where #6 (19 mm), #7 (22.2 mm), or #8 (25.4 mm) bars were used with 50 mm cover.
90 Stirrups consisted of #3 (9.5 mm) bars. Shear wall thickness is taken as 300 mm with #4 (12.7
91 mm), #5 (15.8 mm), or #8 (25.4 mm) reinforcing bars, as required, with 50 mm cover. Concrete
92 strength is taken as 28 MPa, while reinforcing steel yield strength is taken as 414 MPa. The
93 resulting structures are shown in Fig. 1, where column and shear wall locations are indicated on
94 the top floor.

95 **Numerical Model**

96 Structures were modeled with the fully nonlinear, large strain, large displacement finite
97 element-based blast analysis code ELS, which is described elsewhere (ASI 2010; Meguro &
98 Tagel-Din 2002). With the approach implemented in ELS, the ‘applied element method’(AEM),
99 elements are connected by a series of springs on element surfaces, where one normal and two
100 shear springs (one in each direction) are located at each surface contact point, as shown in Fig. 2-
101 a. Spring stiffness varies as a function of stress or strain as given by the material model, and
102 once a specified failure criterion is reached, as discussed below, the springs release element
103 connectivity, which allows efficient simulation of material softening and fracture along element
104 lines. When contact occurs between elements, linear springs are generated at contact points to
105 transfer energy between elements.

106 For concrete, the Maekawa elasto-plastic and fracture model (Maekawa and Okamura
107 1983) is implemented, as shown in Fig. 2-b. In this model, Young’s modulus, the fracture
108 parameter (which defines the extent of existing damage, as a function of the load history), and
109 the current plastic strain are used to define the compressive stresses-strain relationship. Although
110 represented simply as a uniaxial stress-strain relationship in Figure 2-b for illustration, the

111 softening behavior of the concrete is governed by the resulting multi-axial stress state caused by
112 the combination of normal and deviatoric stresses imposed on the element. That is, the state of
113 stress and resulting damage caused by an interaction of axial, shear, and flexural deformations
114 are implicitly accounted for in the model. For the 27.6 MPa compressive strength (f'_c) concrete
115 considered, modulus of rupture (f_r) was taken as 2.6 MPa and modulus of elasticity as 24,800
116 MPa, while shear modulus (G) was taken as 9,650 MPa. These material properties are
117 summarized in Table 1. When concrete is subjected to tension, stiffness is taken as the initial
118 stiffness until the cracking point is reached, at which point the effected spring(s) joining adjacent
119 concrete elements are released. If separated element surfaces contact, the connective springs are
120 regenerated (with zero tension strength). This unloading and reloading behavior is illustrated in
121 Fig. 2-b. Shear behavior is considered linear until cracking strain (as calculated from principle
122 stress) is reached.

123 Strain rate strengthening is frequently accounted for by imposing an empirically
124 developed curve that adjusts strength based on rate of strain (see, for example, Eamon et al.
125 2004). However, in AEM, an alternative approach was implemented. In this method, Poisson's
126 ratio is lowered to zero under high strain rates, preventing the lateral expansion of the material
127 and corresponding creation of lateral cracks (i.e. element separation), essentially strengthening
128 the material under high rates of strain. As detailed by Tagel-Din (2009), this approach was
129 shown to have good agreement to the traditional strain rate curve approach as well as to
130 experimental data.

131 Steel reinforcing bars are modeled explicitly with spring (i.e. bar) elements, in which the
132 nonlinear stress-strain response described by Ristic et al. (1986) governs behavior (Fig. 2-c).
133 Tangent stiffness is calculated based on the state of strain, loading/unloading status and the

134 previous load history, which controls Bauschinger's effect, where rupture is reached once the
135 normal stress is equal to or greater than the ultimate stress of the steel material. The yield and
136 ultimate stresses for steel reinforcement were taken as $f_y = 414$ MPa and $f_u = 538$ MPa,
137 respectively. The steel modulus of elasticity was set equal to 200,000 MPa, with shear modulus
138 of 11,000 MPa. Steel material properties are summarized in Table 1.

139 Often in practice, constraints related to the project schedule, budget, or available
140 computational resources may not allow the blast event and its corresponding pressure-time
141 history to be directly modeled. As such, it is common practice to simply remove a member from
142 the structure to simulate its loss of load-carrying capacity under blast. As noted above, although
143 some studies simulated blast effects in this manner and loaded the resulting structure only with
144 gravity loads, initial analyses conducted for this study found significant differences in structural
145 response between column removal and failing the same column with blast pressure. Specifically,
146 for several structures it was found that a complete collapse resulted when a blast pressure was
147 applied, while no collapse resulted when the same columns were simply removed. In these
148 cases, this difference occurred because the blast load also damaged members near the removed
149 columns as well, significantly weakening the adjoining beams and slab in some cases. Using an
150 assumed spherical (i.e. non-directional) blast charge, it was generally found to be very difficult,
151 if not impossible, to apply sufficient blast pressure that would remove the members of interest,
152 but yet leave adjacent members relatively undamaged from the blast. Therefore, all collapse
153 analyses for this study were initiated using blast pressure. Here, a simplified blast model was
154 used where blast pressures resulting from a spherical TNT charge are calculated using the free-
155 field wave equation based on TM5-1300 (Departments of the Army, Navy, and Air Force 1990).
156 The explosion was taken as an unconfined surface burst, since the detonations were located

157 outdoors and close to the ground (taken approximately 1 m above ground in all analyses), so that
158 the initial shock is amplified at the point of detonation due to the ground reflection. In this case,
159 where the charge height (Z_c) is less than twice the charge radius (R_c), the charge radius is
160 calculated for a spherical shape as:

$$161 \quad R_c = \sqrt[3]{3w/4\Pi\rho_{TNT}} \quad (1)$$

162 where the charge weight (w) is multiplied by a magnification factor,

$$163 \quad M_f = 2.0 - Z_c/0.5R_c \quad (2)$$

164 Here, the TNT charge density (ρ_{TNT}) is taken as 1650 kg/m^3 . The air is considered an
165 ideal gas at sea level and the atmospheric pressure (P_a) = 101,325 Pascal. Based on the charge
166 weights selected (see below), an external blast effect sufficient to cause two adjacent ground
167 floor columns to fail in each model was considered. This was found to be equivalent TNT
168 weights of approximately 340, 590 and 700 kg for the 3, 6, and 10 story buildings, respectively.
169 That is, all structures of the same height, both shear wall and MRF, were exposed to the same
170 charge weight for consistent comparison. This resulted in nearly all of the structures considered
171 (10 story) being exposed to the same equivalent TNT weight of 700 kg. However, for the two 3
172 and 6 story structures considered, charge weights were reduced because the initial 700 kg charge
173 would have resulted in complete destruction of these smaller buildings, due to their substantially
174 lower column capacities, and no difference in performance between MRF and shear wall
175 buildings would be obtainable. It should be noted that the use of different charge weights for
176 these smaller buildings likely corresponds to a different probability of occurrence than for the
177 larger charge weight applied to the 10 story structures, and thus comparisons of safety cannot

178 directly be made between structures of different heights. In this blast model, blast pressures are
179 applied to element surfaces that have a direct line of sight with the TNT charge. It should be
180 noted that the main purpose of the blast analysis was to produce an extreme load that allows
181 reasonable comparison of the response of different structures to possible progressive collapse,
182 rather than to simulate the blast event itself in great detail. Thus, to ease numerical
183 implementation of the comparison, various blast load simplifications were implemented. In
184 particular, the effects of temperature, suction pressure, blast wave reflections on the structure,
185 explosive casing (bare TNT weight only considered), and possible ground motion were
186 neglected. Moreover, all structures are assumed to have a nonstructural façade that is destroyed
187 upon blast impact, before significant additional pressure can be distributed to the structural
188 system. In accordance to the recommendations in USDOD 2002, during the blast load event, the
189 service dead load and 50% of the service live load were applied to the models as lumped masses
190 added to the slabs.

191 The resulting models ranged in size from approximately 55,000-117,000 rectangular solid
192 elements, and were solved using a time step increment of 0.0001 s during the blast stage. For the
193 first two levels of the models, element edge lengths varied from 9-12 cm for columns, 14-20 cm
194 for beams, and 18-30 cm on slabs. For the upper stories, a more coarse mesh was used, with
195 element sizes approximately doubled. Similarly, wall element dimensions ranged from 15-37
196 cm. It was found that the use of a finer mesh resulted in differences in localized fracture
197 patterns, but produced no significant differences in global response, the concern of this study,
198 and thus was not computationally justified. That is, since in the AEM approach, as cracks may
199 only develop and propagate along element boundaries, increasing the number of elements may
200 result in the development of different crack patterns. For example, in some cases, increasing

201 element density results in a larger number of smaller cracks as opposed to a small number of
202 large cracks. Although several alternative crack patterns may sufficiently capture component
203 behavior to accurately model the response of the overall structure, as was found in this study, the
204 crack pattern that results from a more coarse mesh may be insufficient to model phenomenon at a
205 smaller scale (crack geometry, local damage pattern on the component, accurate assessments of
206 curvature and deflected shape, etc.)

207 A smaller time step increment of 0.00001 s was also considered, and was found to
208 produce slightly larger force effects on the structure during the blast stage. However, it was
209 determined that the excessive additional computational effort required for this smaller time step
210 was similarly not justified for this study, as relative differences in performance between the
211 different structures considered were unchanged. Each analysis required approximately 32-54
212 hours of CPU time on a 2.3-GHz quad-core CPU with 8 GB of RAM.

213 **Verification Cases**

214 Experimental verification of the collapse behavior of full-scale, actual buildings
215 subjected to blast is challenging, as few experimental subjects exist. However, in this study, for
216 validation, the analysis approach was used to model the progressive collapse of two actual
217 reinforced concrete buildings subjected to explosive demolition. These structures are the
218 Crabtree Sheraton Hotel located at Raleigh, NC (May, 2006) and Stubbs Tower located at
219 Savannah, GA (December, 2007), for which the structural plans and demolition video footage
220 were obtained. The Crabtree Sheraton Hotel was a 10-story (30 m high) building in a 3 x 9 bay
221 rectangular plan configuration (total plan dimensions 18 m x 36 m) with a two-way flat plate
222 floor system (1800 mm thick). The Stubbs Tower was a 15 story (45 m high) building

223 constructed using two types of loadbearing systems; a column and girder concrete frame system
224 for the first floor and load bearing concrete walls for the remaining floors. The building was
225 structured in a 3 x 16 bay configuration (19 m x 56 m total plan dimensions). Both structures
226 were modeled using the numerical technique discussed above. It was found that the analytical
227 simulations well-matched the progressive collapse behavior of both structures, as shown in Figs.
228 3 and 4. In Fig. 4, vertical displacements were measured from the available video footage of the
229 collapses at the points (V) as indicated in Fig. 3. Therefore, the method was considered
230 sufficiently accurate for the modeling purposes of this study. Other researchers have had similar
231 success with the AEM approach for modeling collapse behavior as well (Kernicky et al. 2014;
232 Salem et al. 2014; Salem 2011; Keys and Clublely 2013; Lupoae et al. 2013).

233 **Results**

234 **Moment Resisting Frame Structures**

235 As the objective of the study is to compare the collapse behavior of different structures
236 subjected to a similar level of damage, for all external blast analyses, the charge position was
237 selected such that two adjacent exterior columns just failed. For all structures, this was
238 approximately 1 m away from the face of the structure, centered between the two central
239 columns, as shown in Fig. 5. With the charge in this position, approximately four seconds after
240 the blast, the 3x3 MRF structure experienced a complete progressive collapse, as shown in Fig.
241 6. Note that, beyond 4.0 s (not shown), all floors of the structure eventually collapsed to the
242 ground.

243 As shown in Fig. 6, the blast first resulted in collapse of the floor slab in the bay adjacent
244 to the charge, which failed from the uplifting blast pressure. Next, the two columns closest to the

245 blast (C2 and C3 in Fig. 7) failed in bending caused by the blast pressure as well as a large
246 increase in moment caused by the axial gravity loads, which became increasingly eccentric to the
247 deformed column mid-section. Once these columns failed, the remaining columns quickly
248 followed. Studying the changes in column forces as a function of time, as shown in Fig. 8, it can
249 be seen that columns C6 and C7 were also directly affected by and failed in bending from the
250 blast pressure, at a slightly delayed time, while columns C1, C4, C5 and C8 failed primarily in
251 compression (actually due to combined compressive and bending effects, but axial compression
252 was greatly dominant) due to redistribution of the gravity loads. This is evident at $t=0.3$ s in Fig.
253 8, where the axial loads in these columns greatly increased once columns C2, C3, C6, and C7
254 lost axial load carrying capacity (i.e. where axial force becomes approximately 0 at $t=0.4$ s in
255 Fig. 8). Note that, the design axial capacity (nominal capacity reduced by the appropriate
256 resistance factor) for exterior columns C1, C4, C5, and C8 is approximately 4,497 kN, while
257 maximum axial loads on these columns varied from 1,780 kN to 4,890 kN at any time in the
258 analysis. However, the interior columns (C6, C7, C10, and C11) have higher design axial
259 capacities of approximately 4,640 kN. Thus, although columns C10 and C11 carried larger
260 amounts of (redistributed) axial load (Fig. 7 at $t=2.05$ s) they did not fail first because their axial
261 capacity is higher than the adjacent exterior columns.

262 The failure times for columns C5, C1, C4, and C8 occurred approximately at 1.2 s, 1.85
263 s, 2.05 s, and 2.2 s, respectively, as shown in Fig. 8, where large, abrupt decreases in axial force
264 in the column occurs. These failure times correspond to the times for which the axial force
265 diagrams are constructed in Fig. 7. An examination of column moments indicates that bending
266 moment was not a main reason for the failure of most columns (exceptions: C2, C3, C6, and C7,
267 which were closest to the blast), since the moment capacity was generally not exceeded in the

268 analysis. For example, for columns C1, C4, C5, and C8, the moment capacity is approximately
269 270 kN-m, while maximum moments on these columns did not exceed 136 kN-m during the
270 analysis.

271 For the corresponding 4x4 MRF structure, approximately 2.5 s after charge detonation, a
272 major progressive collapse occurred, as shown in Fig. 9-c. The collapse behavior for the 4x4 and
273 3x3 MRF structures was similar, where axial loads carried by damaged columns nearest to the
274 blast were redistributed to the remaining columns, causing progression of the collapse.

275 Considering the 5x5 MRF structure, approximately 4 s after charge detonation, severe
276 local damage near the blast location occurred (slab and column failure), but the structure did not
277 collapse, as shown in Fig. 10. Similar to the 3x3 structure, once a local failure occurred, a more
278 extensive redistribution of axial loads followed throughout the 5x5 frame due to the greater
279 number of available members. Although the members furthest away from the blast received
280 relatively little load, this surrounding structural system was an important influence on overall
281 system behavior. These surrounding members not only reduced the redistributed axial loads
282 further, but also provided additional constraint and stability for the most heavily loaded portions
283 of the structure, preventing progressive collapse.

284 In this structure, the time-displacement curve of a point at the top of the most severely
285 damaged column (C3) shows that the maximum downward vertical (Z) displacement was
286 approximately 127 mm at $t=2.9$ s. After $t=2.9$ s, no significant additional vertical displacement
287 occurred, as shown in Fig. 10. The horizontal displacement in the direction parallel to the blast
288 direction (X) shows the structure vibrating with a period of approximately 1.5-2 s, while the
289 horizontal displacement perpendicular to the blast (Y) shows no significant motion after column
290 C3 failed (due to blast). These small changes in horizontal and vertical displacements after the

291 failure of Columns C2, C3 and C4 indicate the sustained stability of the structure. Columns just
292 adjacent to the failed columns (C2, C3 and C4) carried the majority of the redistributed axial
293 forces from the failed columns, but as noted above, the larger number of members surrounding
294 the damaged columns allowed for successful load redistribution and continuing stability.
295 Overall, as expected, the analyses of the three MRF structures indicate that increasing the
296 number of bays results in a more successful redistribution of axial loads over the remaining
297 stable structure components once a local collapse has been initiated.

298 **Shear Wall Structures**

299 For the 3x3 shear wall structure, after running the analysis for approximately 5.0 s, a
300 major progressive collapse resulted. However, the remaining shear wall core remained stable, as
301 shown in Fig. 11.

302 The axial forces carried by the major structural components are given in Fig. 12. As
303 shown, the shear walls carry approximately 54% (27,179 kN) of the total axial load (50,265 kN)
304 at $t=2.0$ s. Clearly, they have a significant influence on axial force distribution. During the
305 analysis, columns C1, C2, C3, and C4 failed first, then, as shown in Fig. 13, the failure of
306 columns C6 and C7 occurred simultaneously with the partial failure of shear wall S1 at
307 approximately $t=1.8$ s (due to direct blast pressure). The failure of these components then
308 increased the axial loads on the remaining shear walls S2, S3 and S4, which occurs at
309 approximately $t=1.8$ s in Fig. 13. At approximately $t=2.5$ s, the impact of the falling slabs with
310 the damaged shear wall S1 (Fig. 11) caused a large increase in the axial force in shear wall S3 as
311 S1 failed completely, while simultaneously, shear walls S2 and S4 experienced a large decrease
312 in axial force, as shown in Fig. 13. This occurs because the impact of the floor slabs into the
313 shear wall tower was accompanied by a large lateral (impact) load. Conceptually, after the

314 failure of S1, the remaining shear wall structure acted similar to a cantilever beam, fixed at
315 ground level, with a U-shape in section, where S3 acted as the compression flange and S2 and S4
316 as the tension webs. However, the remaining shear walls remained stable after $t=5.0$ s in the
317 analysis, since the failure of the slabs also resulted in removal of the axial loads that they had
318 previously transferred to the shear walls.

319 For the 4x4 shear wall structure, in approximately 4.5 s, a progressive collapse of about
320 50% of the structure occurred, but the collapse stopped at the location of the shear walls. Here,
321 the shear walls provided the structure with significant stability, as shown in Fig. 14. In this
322 structure, the floor slabs in the bays adjacent to the charge first failed from the uplifting blast
323 pressure. Simultaneously, the closest columns to the charge (C1-C4 and C7) failed in bending
324 caused by the blast pressure. Once these exterior columns failed, the floor slabs which they
325 supported toppled onto adjacent first floor columns, causing their failure (see $t=2.5$ s in Fig. 14).
326 However, progressive collapse of the floor slabs was halted at the location of the shear walls,
327 preventing failure of the remaining columns.

328 In addition, the shear walls were able to carry a significant portion of the axial load that
329 was previously carried by the damaged columns. The axial force curves in Fig. 15 show how the
330 shear walls (S1, S2, S3 and S4) and the columns (C8, C12, C14 and C18) at the ends of the shear
331 walls shared the axial loads in a way that reduced excessive axial loads on these columns. For
332 example, from $t=0.3$ s to approximately $t=0.75$ s, as the structure sways, we can observe that S1,
333 S4, C8 and C12 (Group 1) are subjected to an increase in axial loads, while S2, S3, C14 and C18
334 (Group 2) are subjected to a decrease in axial loads. This behavior is reversed after $t=0.75$ s,
335 where Group 1 components are subjected to a decrease in axial loads, while Group 2 components
336 are subjected to an increase in axial loads. Clearly, the columns and shear walls act efficiently

337 together as two distinct groups of components, sharing the axial loads. The sway of the shear
338 wall core can be seen more clearly in Fig. 16, where walls and columns facing the blast (walls
339 S1, S4 and columns C8, C12) have highest compression at the times when walls and columns
340 opposite the blast (walls S2, S3 and columns C14, C18) have lowest compression.

341 For the 5x5 shear wall structure, although a collapse began upon detonation, similar to
342 the other shear wall structures, the progressive collapse stopped at the shear walls, as shown in
343 Fig. 18-b (at $t=5.0$ s). The behavior of the shear walls of the 5x5 model was very similar to that
344 of the shear walls of the 4x4 model. In both models, the walls carried a significant amount of
345 axial load, which reduced the magnitude of the redistributed axial loads to the columns adjacent
346 to those that failed. This resulted in halting the progression of the collapse. Moreover, a
347 secondary effect of the presence of the shear walls is that they contributed significantly to aid in
348 blocking falling debris and slabs from striking and damaging the remaining stable components of
349 the structure.

350 **Effect of Building Height**

351 To examine the effect of building height on collapse performance, the 4x4 structure was
352 redesigned with 3 and 6 story configurations, where column and shear wall capacities were
353 altered as discussed above. It was found that as building height decreased, overall collapse
354 behavior was similar to that of the 10 story structures, as shown in Figs. 9, 17-a, and 17-b.
355 However, the charge weight needed to fail two exterior columns, and correspondingly initiate
356 collapse, decreased for the lower height buildings. For the 3 story building, a charge weight of
357 340 kg, approximately half that needed to initiate collapse of the 10 story building, resulted in
358 total collapse. For the 6 story building, a charge weight of 590 kg was required to initiate
359 collapse. Such results are not unexpected, since ground floor column capacity decreases with

360 decreasing building height. Quantitatively, it was found that the ratio of charge weights needed
361 to fail the different height structures fell within the ratio of column capacities for axial force and
362 moment. Specifically, for the 6 story building, the ratios of: a) column nominal axial capacity to
363 that of the 3 story structure, followed by b) charge weight needed to fail the buildings, and c)
364 column nominal moment capacities, are: (1.2, 1.7, 3.0). Similarly, ratios for the 10 story to the 3
365 story structure are: (1.8, 2.1, 3.6).

366 It should also be noted that as height increased, a slight delay in the collapse progression
367 occurred. As shown in Figs. 9, 14, and 17, the rate of collapse progression was highest and
368 lowest for the three and ten story structures, respectively. For example, in Fig. 9, two stories of
369 the 3 story structure partially collapsed at the same time (1.5 s) that 1 story of the 6 story
370 structure and no stories in the 10 story structure partially collapsed.

371 **Effect of Shear Wall Location**

372 To study the effect of shear wall location, two additional configurations were considered
373 for the 4x4 and 5x5 10 story structures. These additional configurations explored the effect of
374 moving the shear walls from the original central location to progressively more dispersed
375 arrangements. As shown in Figs. 17-c and 17-d (compared to Fig. 14), for the 4x4 structure,
376 changing shear wall arrangement had minimal effect on overall behavior, as in each case,
377 collapse of a significant portion of the structure resulted. As shown, it was also found that
378 separating the shear walls resulted in failure of one of the walls closest to the blast. For the 5x5
379 structure, however, separating and moving the shear walls to the exterior of the building (which
380 were placed perpendicular to the facade, to avoid blocking potential fenestration) resulted in
381 greatly minimizing damage from the blast, and resisted system collapse (Fig. 18-c). Thus, it
382 appears that shear wall placement may have a significant influence on collapse resistance, but the

383 effect is highly dependent on building geometry and component strength. By consideration of
384 shear wall and charge placement, the models were specifically constructed to locate the blast
385 charge as far as possible from the shear walls, while attempting to maintain somewhat symmetric
386 and reasonable wall placement schemes. This was done to minimize the potential shielding
387 effect from the blast load that the shear walls may provide the columns, and also to minimize the
388 beneficial effect of placing a high capacity structural element close to the blast source, which can
389 more readily support the loads redistributed by failed columns. However, these effects cannot be
390 eliminated completely, and are contributing factors to the performance of shear wall buildings.
391 A secondary effect of the presence of the shear walls is that they contributed significantly to aid
392 in blocking falling debris and slabs from striking and damaging the remaining stable components
393 of the structure.

394 **Effect of Charge Location**

395 To study the effect of charge placement, the 10 story 4x4 structure was again considered.
396 In this case, two additional analyses were conducted where the 700 kg charge that caused
397 collapse when placed at the building exterior was progressively moved inward toward the center
398 of the building. Charges were placed 1 m above the ground level, either 1 m from the center
399 column or at the center of the corner bay of each structure, as shown in Fig. 19. For the MRF
400 structures (Figs. 19-a and 19-b), changing charge location had no significant effect on behavior,
401 where similar, complete collapse behavior resulted regardless of charge position. For the shear
402 wall structure (Figs. 19-c and 19-d), moving the charge into the center of a corner bay resulted in
403 a similar level of destruction as the original external charge location. However, when the charge
404 was placed near the center of the building, insignificant damage to the structural system
405 occurred. This is because the shear wall, although it experienced complete local removal of

406 material by the blast, maintained sufficient resistance in the surrounding material to avoid
407 collapse. Such a result suggests that a reasonably reinforced bearing wall structure has the
408 potential to experience greater blast resistance than an equivalent frame structure.

409 **Summary and Conclusions**

410 In this study, the effect of the type of lateral load resisting system on reinforced concrete
411 structure resistance to progressive collapse when exposed to blast load was examined using an
412 existing finite element approach. The modeling technique employed was found to reasonably
413 replicate the collapse behavior of two actual structures subjected to blast demolition for which
414 data are available. Using this validated modeling approach, fourteen different reinforced
415 concrete structures were considered for analysis, with five structures designed as moment
416 resisting frames and nine designed as shear walls systems. Buildings with 3, 6, and 10 stories
417 with 3, 4, and 5-bay symmetric configurations were considered. Charge weights required to fail
418 two exterior columns in all structures varied from 340-700 kg, depending on building height,
419 where lower height structures required the lower charge weights.

420 Under the blast loads considered, which were sized to just remove two exterior columns,
421 the 10 story 3x3 and 4x4 MRF structures experienced complete collapse, while the 5x5 building
422 suffered local damage only. In contrast, the performance of the shear wall buildings was
423 dependent upon building size and shear wall placement. The 3x3 structure, with shear walls
424 placed in the core of the building, resulted in complete collapse, with major damage to the shear
425 walls. Regardless of shear wall placement, the 4x4 building experienced a partial collapse of
426 approximately half of the structure, where the collapse progression halted at the shear walls. The
427 5x5 structure resulted in complete, partial, and no collapse, when shear walls were placed at the
428 core, within middle bays, and within exterior bays of the structure, respectively.

429 Building height had little effect on overall performance once two exterior columns failed.
430 All of the 3, 6, and 10 story MRF buildings resulted in complete collapse, while each of the 4x4
431 shear wall structures resulted in a partial collapse of approximately half of the building, which
432 stopped at the location of the shear walls. Another parameter explored was blast location, where
433 interior as well as exterior blasts resulted in complete collapse of the 4x4 MRF structure.
434 However, a partial and no collapse resulted for the corresponding shear wall structure when the
435 charge was placed within an exterior and a core bay, respectively.

436 Results for all analyses are summarized in Table 2, where the percent of collapsed floor
437 area (“% collapsed”) and the corresponding collapsed area per charge weight (“CA/TNT”, in
438 m²/kg) are given. In the Table, models are designated with the bay configuration followed by
439 height in stories, while labels “a”, “b”, and “c” refer to shear wall configurations as shown in
440 Figs. 17-b, c, and d, respectively, for 4x4 models, and as shown in Figs. 18-a, b, and c,
441 respectively, for 5x5 models. Finally, labels “i” and “e” refer to analyses where the charge was
442 placed inside the structure, near the interior (i) and exterior (e), respectively, as shown in Fig. 19.
443 Following the model label, the charge weight used is given in parenthesis (kg). As shown in
444 Table 2, in terms of percent of floor area lost, all MRF structures except for the 5x5-10 model
445 resulted in complete collapse, while none of the shear wall structures were fully destroyed.
446 Although the range of destruction was large (from 1-96% collapsed), the average floor area loss
447 was approximately 52%, with most values ranging from about 44-63%, substantially less than
448 the typical 100% loss for corresponding MRF buildings. Correspondingly, average CA/TNT
449 values were 5.3 for shear wall structures and 8.3 for MRFs, indicating that the MRFs were
450 subjected to greater damage on an area lost per unit charge weight basis.

451 Of all parameters studied, in general, it was found that two were most significant on
452 reducing potential for progressive collapse under blast loading; building size and shear wall
453 placement. With regard to building size, as demonstrated in the analyses, larger structures carry
454 two possible advantages. For building larger in plan, greater redundancy allows for increased
455 load sharing ability among remaining structural members, potentially limiting surviving member
456 overload and corresponding failure. For buildings larger in height, the associated increase in
457 member capacities supply a larger capacity to resist blast load, requiring a larger charge weight
458 to severely damage the structure. Moreover, as building plan as well as height increases,
459 additional structural elements are available to allow bridging over damaged areas. With regard
460 to shear wall placement, overall, it was found that moving the walls as close to the exterior bays
461 as possible resulted in a greater resistance to progressive collapse. One reason for this is the
462 associated increase in the moment of inertia of the building plan, allowing the structure as a
463 whole to more effectively carry unbalanced axial loads caused by damaged columns. Here, with
464 the exception of a shear wall destroyed by the blast, the progressive collapse generally stopped at
465 the remaining shear walls.

466 Based on the results of this study, simply increasing first floor member capacities was
467 found to be an effective way to significantly increase structural resistance to blast. As shown, for
468 the structures considered, proportional increases of charge weight resisting ability roughly
469 mirrored proportional increases in column strength. Along with increases in column strength, a
470 larger building plan similarly demonstrated enhanced resistance to progressive collapse. Such
471 construction might be justified architecturally by considering one large structure in favor of
472 several smaller structures, for example. Second, the use of dispersed shear walls, where walls
473 are placed in multiple locations near the building exterior, resulted in superior resistance to

474 progressive collapse than placing shear walls at the building core. This approach, however, will
475 likely cause tension between structural and architectural objectives, where one of the latter is
476 generally to place shear walls inward near the building core. Additional consideration might be
477 given to constructing a safe room for building occupants adjacent to a shear wall. The practice
478 of placing stairwells within a shear wall core or adjacent to a shear wall may be ideal, allowing
479 building occupants a stable passage of escape in the case of a blast emergency.

480

481

482

483

484

485

486

487

488

489

490

491

492

493

494

495

496

497

498

499 **References**

- 500 ACI (American Concrete Institute). (2011). "Building code requirements for structural concrete
501 and commentary." *ACI 318-11*, Farmington Hills, MI.
- 502 Alashker, Y., Li, H., and El-Tawil, S. (2011). "Approximations in progressive collapse
503 modeling." *J. Struct. Eng.*, 10.1061/ (ASCE) ST.1943-541X.0000452, 914-924.
- 504 Almusallam, T. H., Elsanadedy, H. M., Abbas, H., Alsayed, S. H., & Al-Salloum, Y. A. (2010).
505 "Progressive collapse analysis of a RC building subjected to blast loads." *Structural*
506 *Engineering and Mechanics*, 36(3), 301-319.
- 507 ASCE (American Society of Civil Engineers). (2010), "Minimum design loads for buildings and
508 other structures." *SEI/ASCE 7-10*, Reston, Va.
- 509 Applied Science International (ASI), LLC. (2010). Applied Science International, Durham,
510 North Carolina.
- 511 Asprone, D., Jalayer, F., Prota, A., & Manfredi, G. (2010). "Proposal of a probabilistic model for
512 multi-hazard risk assessment of structures in seismic zones subjected to blast for the limit
513 state of collapse." *Structural Safety*, 32(1), 25-34.
- 514 Bažant, Z. and Zhou, Y. (2002). "Why did the world trade center collapse?—simple analysis." *J.*
515 *Eng. Mech.*, 10.1061/ (ASCE) 0733-9399(2002)128:1(2), 2-6.
- 516 Department of Defense (DOD). (2002). "DOD minimum antiterrorism standards for buildings".
517 Unified Facilities Criteria (UFC), UFC 4-010-01. U.S. Army Corps of Engineering,
518 Washington, DC.
- 519 Department of Defense (DOD). (2005). "Design of buildings to resist progressive collapse."
520 Unified Facilities Criteria (UFC) 4-023-03.
- 521 Departments of the Army, the Navy, and the Air Force. (1990). "Structures to resist the effects of
522 accidental explosions." *TM5-1300*.

523 Eamon, C., Baylot, J., and O'Daniel, J. (2004). "Modeling concrete masonry walls subjected to
524 explosive loads." *J. Eng. Mech.*, 10.1061/ (ASCE) 0733-9399(2004)130:9(1098), 1098-
525 1106.

526 El-Tawil, S. and Kuenzli, C. (2002). "Pushover of hybrid coupled walls. II: Analysis and
527 behavior." *J. Struct. Eng.*, 10.1061/ (ASCE) 0733-9445(2002)128:10(1282), 1282-1289.

528 General Services Administration (GSA), (2003), "Progressive collapse analysis and design
529 guidelines for new federal office buildings and major modernization projects." Washington,
530 DC.

531 Granger, R. O., Peirce, J. W., Protze, H. G., Tobin, J. J., & Lally, F. J. (1971). "The building
532 collapse at 2000 Commonwealth Avenue, Boston, Massachusetts, on January 25, 1971."
533 Rep. of the Mayor's Investigating Commission, Boston, Ma.

534 Grierson, D. E., Xu, L., & Liu, Y. (2005). "Progressive-failure analysis of buildings subjected to
535 abnormal loading." *Computer-Aided Civil and Infrastructure Engineering*, 20(3), 155-171.

536 Gross, J. and McGuire, W. (1983). "Progressive collapse resistant design." *J. Struct. Eng.*,
537 10.1061/ (ASCE) 0733-9445(1983)109:1(1), 1-15.

538 Hamburger, R., & Whittaker, A. (2004). "Design of steel structures for blast-related progressive
539 collapse resistance." *Modern Steel Construction*, 44(3), 45-51.

540 Hong, H., Chengqing, W., Zhongxian, L., & AK, A. (2006). "Numerical analysis of structural
541 progressive collapse to blast loads." *Transactions of Tianjin University*, S1.

542 Kernicky, T., Whelan, M., Weggel, D., and Rice, C. (2014). "Structural identification and
543 damage characterization of a masonry infill wall in a full-scale building subjected to internal
544 blast load." *J. Struct. Eng.*, 10.1061/ (ASCE) ST.1943-541X.0001158, D4014013.

545 Keys, R. and Clubley, S. (2013). "Modeling debris distribution of masonry panels subject to
546 blast loads using experimental & applied element methods." Proc., 15th International
547 Symposium on Interaction of the Effects of Munitions (ISIEMS 15), Potsdam, DE, 17–20.

548 Kim, J. K., Lee, Y. H., & Choi, H. H. (2008). "Progressive collapse resisting capacity of braced
549 frames." Journal of the Computational Structural Engineering Institute of Korea, 21(5), 429-
550 437.

551 Korol, R. M., Sivakumaran, K. S., & Greening, F. R. (2011). "Collapse Time Analysis of Multi-
552 Story Structural Steel Buildings." The Open Civil Engineering Journal, 5(1).

553 Li, Z., & Shi, Y. (2008). "Methods for progressive collapse analysis of building structures under
554 blast and impact loads." Transactions of Tianjin University, 14, 329-339.

555 Lupoae, M., Baciuc, C., & Constantin, D. (2013). "Theoretical and experimental research on
556 progressive collapse of RC frame buildings." Urbanism. Arhitectur. Constructii, 4(3), 71-87.

557 Lynn, K. M., & Isobe, D. (2007). "Structural collapse analysis of framed structures under impact
558 loads using ASI-Gauss finite element method." International Journal of Impact Engineering,
559 34(9), 1500-1516.

560 Maekawa, K., & Okamura, H. (1983). "The deformational behavior and constitutive equation of
561 concrete using the elasto-plastic and fracture model." Journal of the Faculty of Engineering,
562 University of Tokyo. Series B, 37(2), 253-328.

563 Málaga-Chuquitaype, C., Elghazouli, A. Y., & Enache, R. (2016). "Contribution of secondary
564 frames to the mitigation of collapse in steel buildings subjected to extreme loads." Structure
565 and Infrastructure Engineering, 12(1), 45-60.

566 Meguro, K. and Tagel-Din, H. (2001). "Applied element simulation of RC structures under
567 cyclic loading." J. Struct. Eng., 10.1061/ (ASCE) 0733-9445(2001)127:11(1295), 1295-
568 1305.

569 Powell, G. (2005). "Progressive collapse: Case studies using nonlinear analysis." Proc.,
570 Metropolis & Beyond: Structures Congress and Forensic Engineering Symposium, New
571 York, NY.

572 Ristic, D., Yamada, Y., & Iemura, H. (1986). "Stress-strain based modeling of hysteretic
573 structures under earthquake induced bending and varying axial loads." Research Rep. No.
574 86-ST, 1.

575 Salem, H. (2011). "Computer-aided design of framed reinforced concrete structures subjected to
576 flood scouring." Journal of American Science, 7(10), 191-200.

577 Salem, H., Mohssen, S., Kosa, K., & Hosoda, A. (2014). "Collapse analysis of Utatsu Ohashi
578 Bridge damaged by Tohoku Tsunami using applied element method." Journal of Advanced
579 Concrete Technology, 12(10), 388-402.

580 Sasani, M., & Sagioglu, S. (2008). "Progressive collapse of reinforced concrete structures: a
581 multihazard perspective." ACI Structural Journal, 105(1), 96.

582 Sasani, M., Kazemi, A., Sagioglu, S., and Forest, S. (2011). "Progressive collapse resistance of
583 an actual 11-story structure subjected to severe initial damage." J. Struct. Eng., 10.1061/
584 (ASCE) ST.1943-541X.0000418, 893-902

585 Tagel-din, H. (2009) "High fidelity modeling of building collapse with realistic visualization of
586 resulting damage and debris using the applied element method." Rep. No. HDTRA1-09-P-
587 0006. Department of Defense.

588 Wierzbicki, T., & Teng, X. (2003). "How the airplane wing cut through the exterior columns of
589 the World Trade Center." *International journal of impact engineering*, 28(6), 601-625.

590 Xu, J. X., & Liu, X. L. (2009). "A two-step approach to progressive collapse analysis of building
591 structures under blast loading." *Journal of Shanghai Jiaotong University (science)*, 14, 393-
592 397.

593 Zhang, Y. M., Sun, C. J., Su, Y. P., & Su, J. Y. (2010). "Finite element analysis of vertical
594 continuous collapse of six-story frame structure." *Applied Mechanics and Materials*, 34,
595 1800-1803.

596 Xu, J. X., & Liu, X. L. (2009). "A two-step approach to progressive collapse analysis of building
597 structures under blast loading." *Journal of shanghai jiaotong university (science)*, 14(4),
598 393-397.

599 Zhang, Y. M., Sun, C. J., Su, Y. P., & Su, J. Y. (2010). "Finite Element Analysis of Vertical
600 Continuous Collapse of Six-Story Frame Structure." *Applied Mechanics and Materials*, 34,
601 1800-1803.

602

603

604

605

606

607

608

609

610

611

612 **List of Figures:**

613

614 **Fig. 1.** Primary Ten Story Structures Considered for Analysis

615 **Fig. 2.** (a) Concept of Element Connectivity Using AEM; (b) Concrete Model; (c) Steel Model

616 **Fig. 3.** Comparisons Between Actual Collapse Results and Simulation: (a) Crabtree Sheraton

617 Hotel, Raleigh, NC; (b) Stubbs Tower, Savannah, GA

618 **Fig. 4.** Time-Displacement Response Comparison

619 **Fig. 5.** Blast Analysis Configuration

620 **Fig. 6.** Response of 3x3 MRF Structure

621 **Fig. 7.** First Floor Column Axial Forces (kN) for 3x3 MRF Structure

622 **Fig. 8.** Column Axial Forces as a Function of Time (3x3 MRF)

623 **Fig. 9.** Response of 4x4 MRF Structures: (a) 3 Stories; (b) 6 Stories; (c) 10 Stories

624 **Fig. 10.** Displacement at Top of Column C3 for the 5x5 MRF Structure

625 **Fig. 11.** Response of 3x3 Shear Wall Structure

626 **Fig. 12.** Shear Wall Axial Load Contribution

627 **Fig. 13.** Shear Wall and Column Axial Forces as a Function of Time (3x3 SW)

628 **Fig. 14.** Response of 4x4 Shear Wall Structure

629 **Fig. 15.** Shear Wall and Column Axial Forces as a Function of Time (4x4 SW)

630 **Fig. 16.** Shear Wall Cyclic Dynamic Response as a Function of Time (4x4 SW)

631 **Fig. 17.** Response of 4x4 Shear Wall Structure: (a) 3 Stories; (b) 6 Stories; (c & d) 10 Story

632 Alternate Shear Wall Configurations

633 **Fig. 18.** Response of 5x5 Shear Wall Structures

634 **Fig. 19.** Internal Blast Responses of 4x4 MRF and SW Structures

635

636

637 **Table 1.** Material Properties (MPa)

Material Property		Concrete	Steel
Compressive strength	f'_c	27.6	-
Modulus of rupture	f_r	2.6	-
Modulus of elasticity	E	24,800	200,000
Shear modulus	G	9,650	11,000
Yield stress	f_y	-	414
Ultimate stress	f_u	-	538

638

639

640 **Table 2.** Summary of Analysis Results

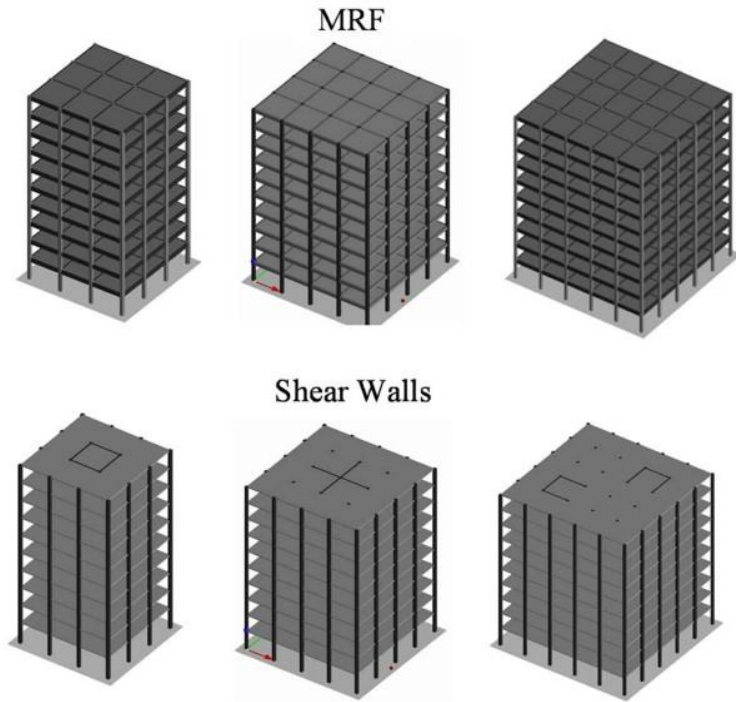
641

Model	Shear Wall		MRF	
	% collapsed	CA/TNT	% collapsed	CA/TNT
4x4-3 (340)	50	8.7	100	17.5
4x4-6 (590)	68	6.9	100	10.1
3x3-10 (700)	89	4.2	100	4.8
4x4-10.a (700)	50	4.2		
4x4-10.b (700)	63	5.3	100	8.5
4x4-10.c (700)	56	4.8		
5x5-10.a (700)	96	12.7		
5x5-10.b (700)	44	5.8	0.4	0.1
5x5-10.c (700)	16	2.1		
4x4-10.i (700)	0.6	0.1	100	8.5
4x4-10.e (700)	44	3.7	100	8.5

642

643

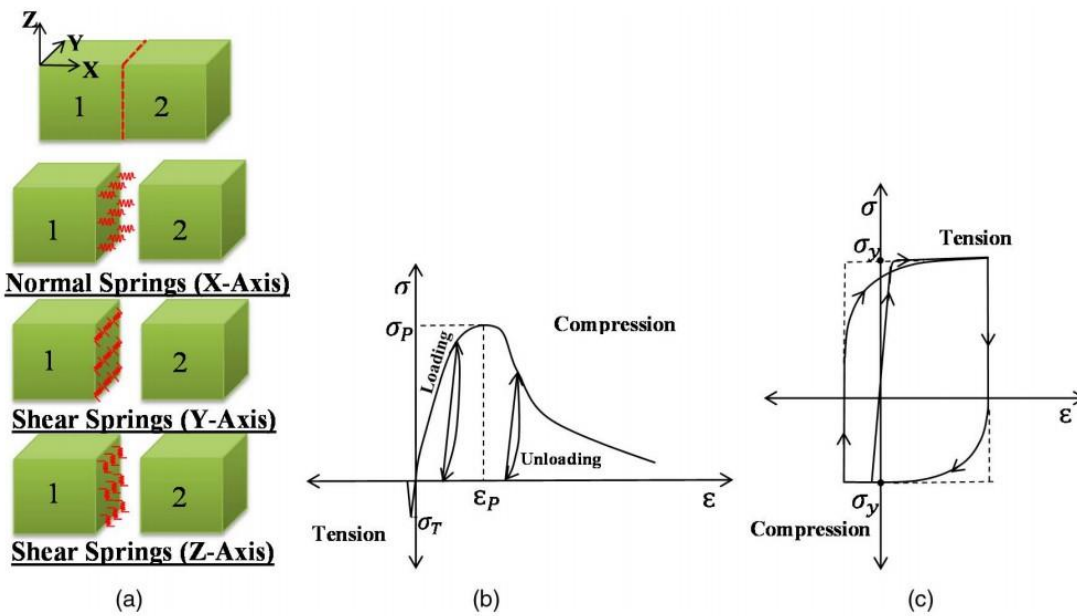
644



645
646 **Fig. 1.** Primary Ten Story Structures Considered for Analysis

647

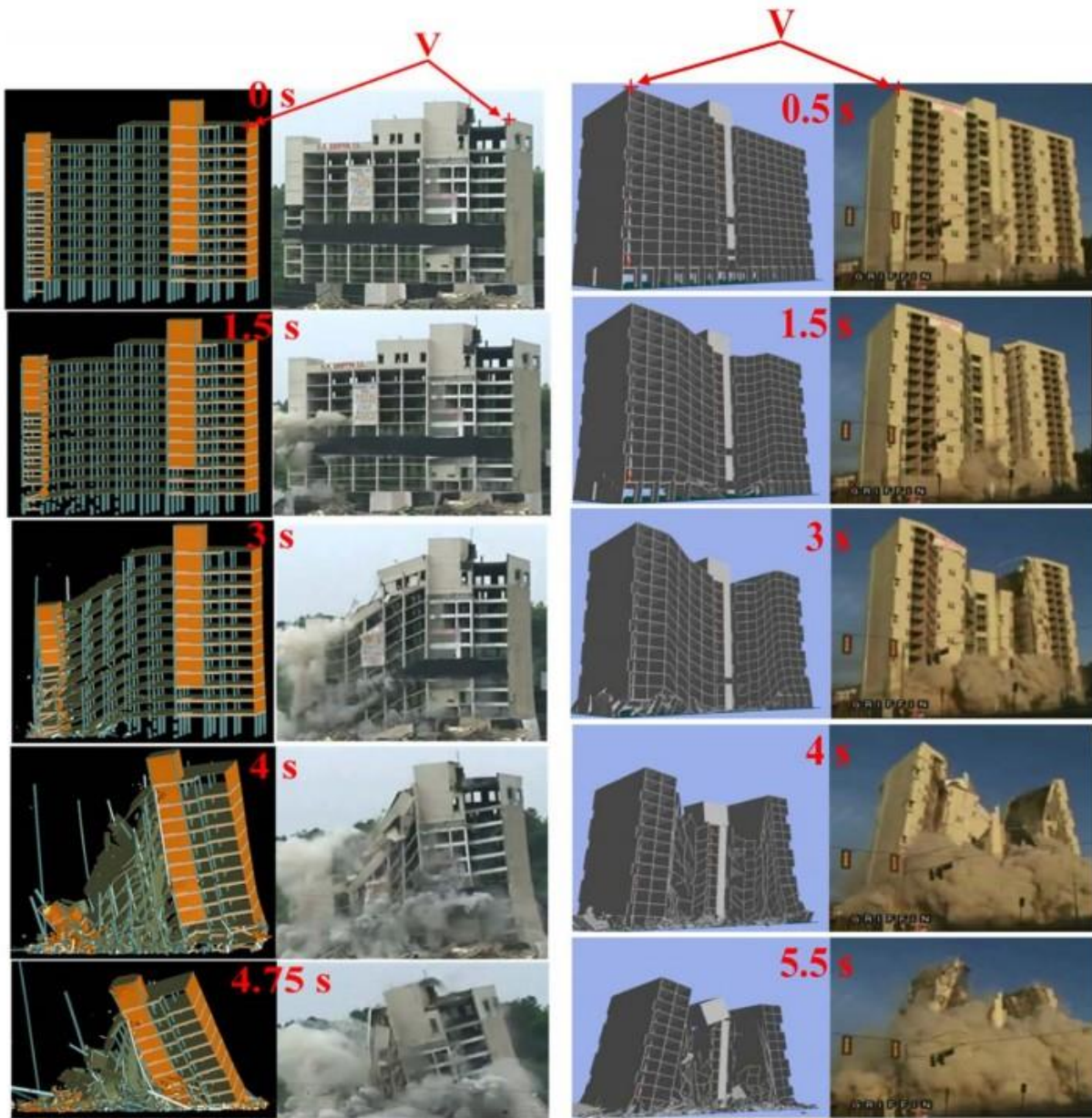
648



649

650 **Fig. 2.** (a) Concept of Element Connectivity Using AEM; (b) Concrete Model; (c) Steel Model

651



(a)

(b)

652

653 **Fig. 3.** Comparisons Between Actual Collapse Results and Simulation: (a) Crabtree Sheraton

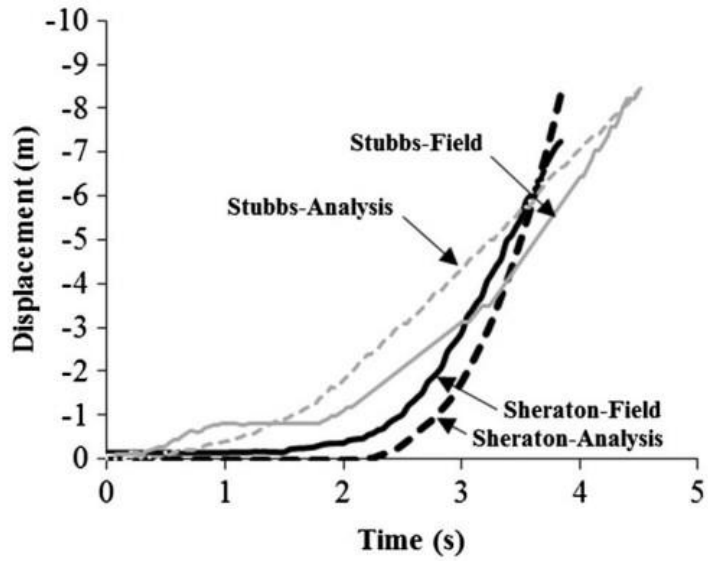
654 Hotel, Raleigh, NC; (b) Stubbs Tower, Savannah, GA

655

656

657

658

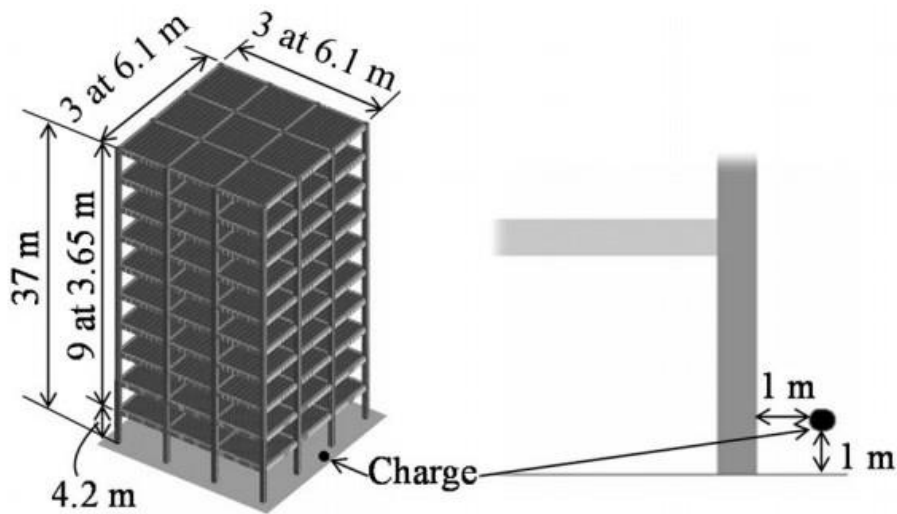


659

660 **Fig. 4.** Time-Displacement Response Comparison

661

662

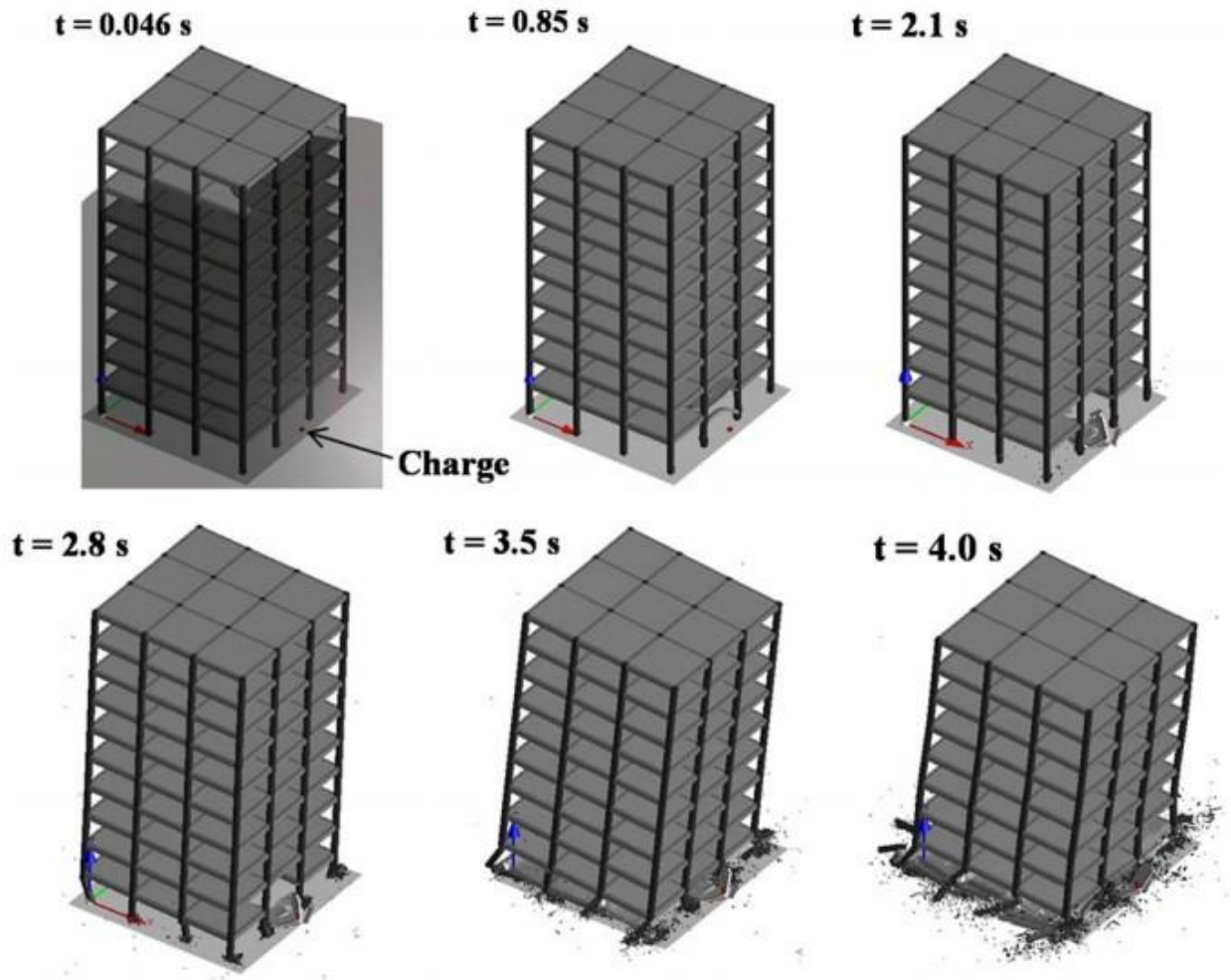


663

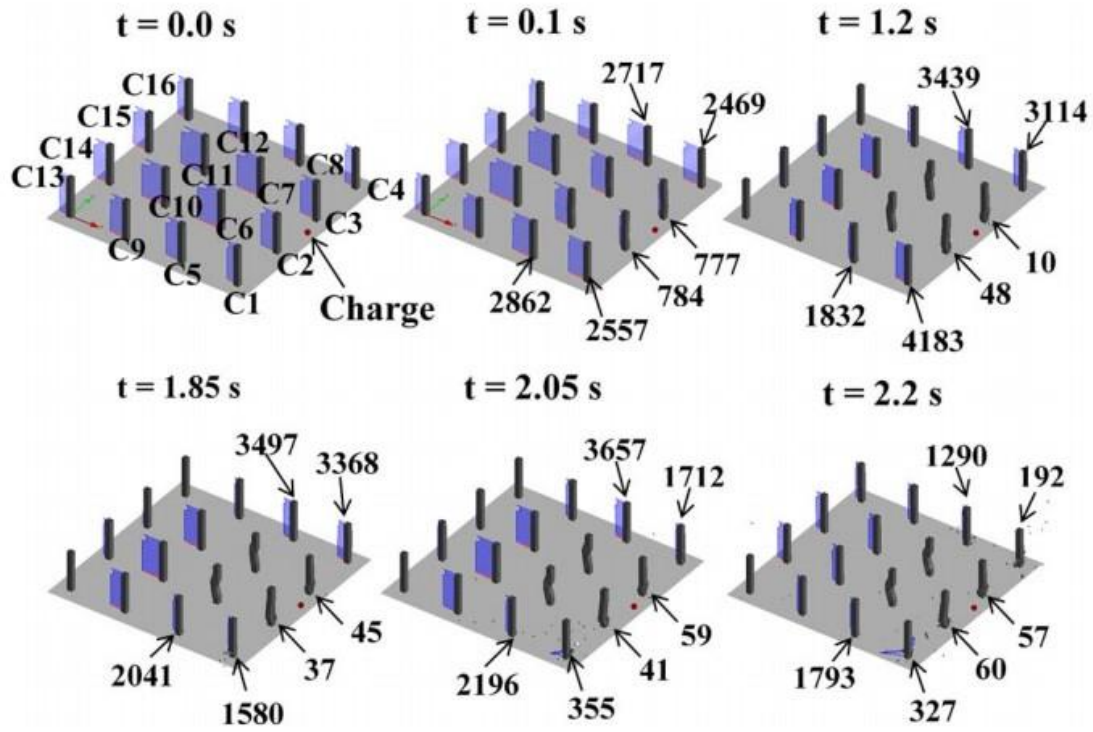
664 **Fig. 5.** Blast Analysis Configuration

665

666



669 **Fig. 6.** Response of 3x3 MRF Structure

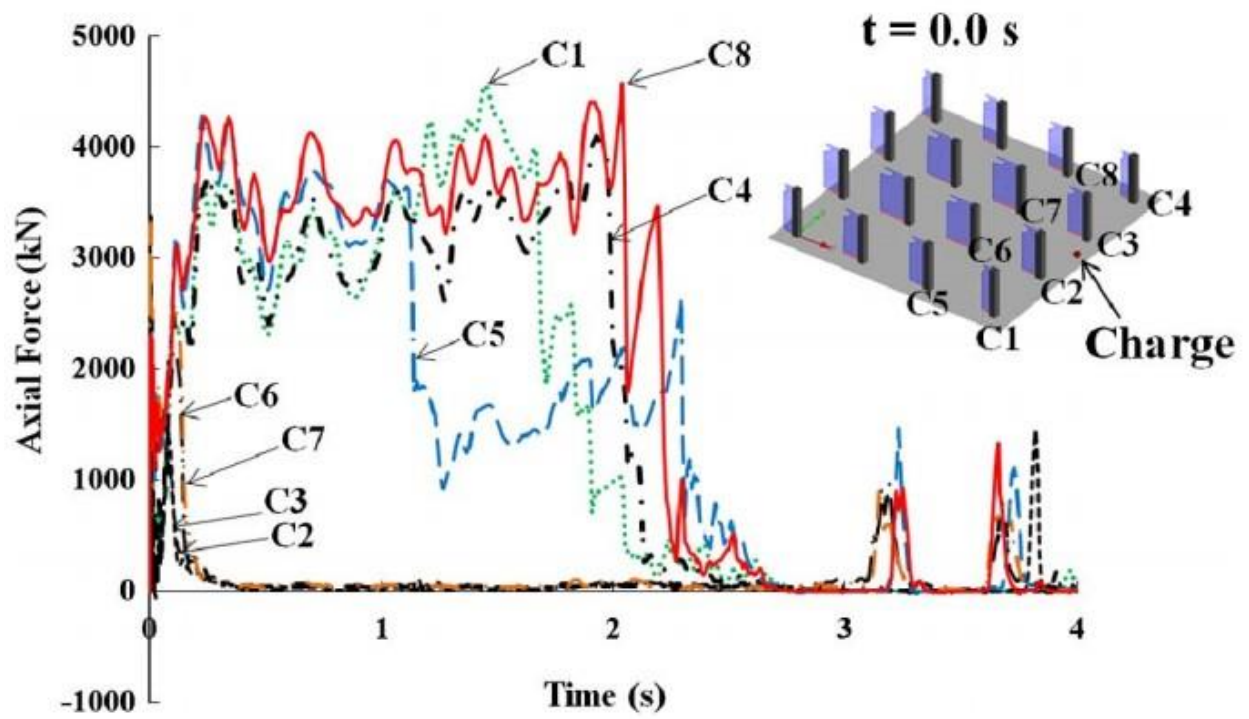


673

674 **Fig. 7.** First Floor Column Axial Forces (kN) for 3x3 MRF Structure

675

676

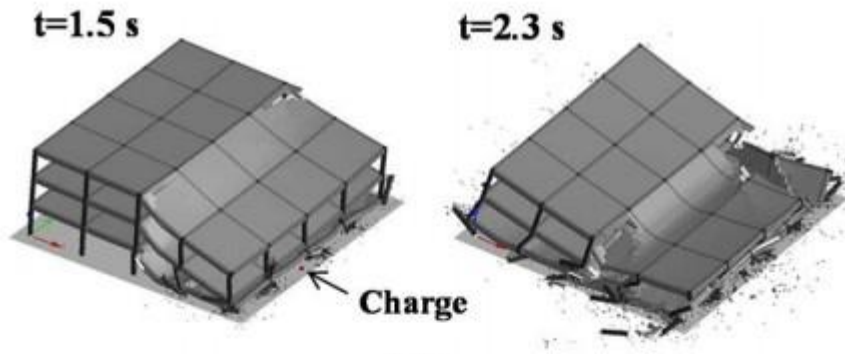


677

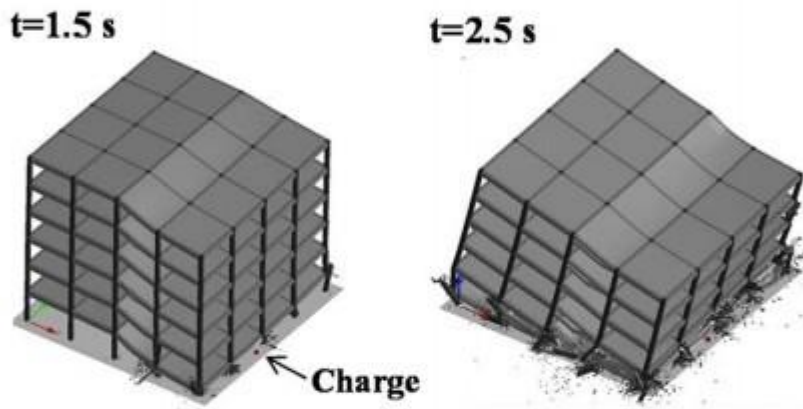
678 **Fig. 8.** Column Axial Forces as a Function of Time (3x3 MRF)

679

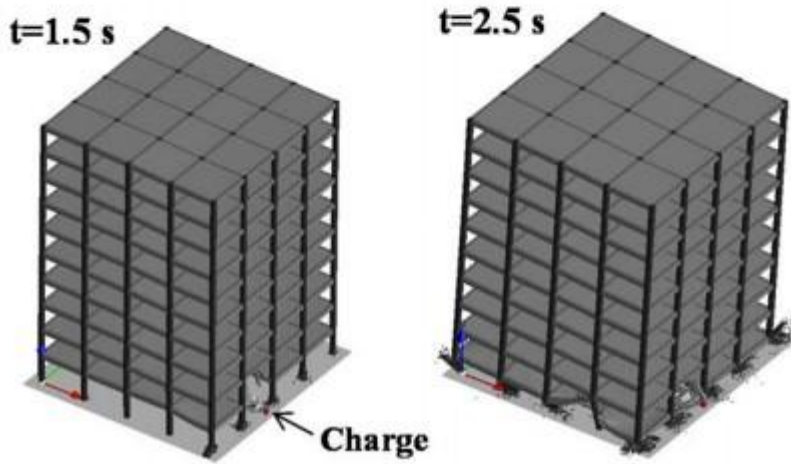
680



(a)



(b)



(c)

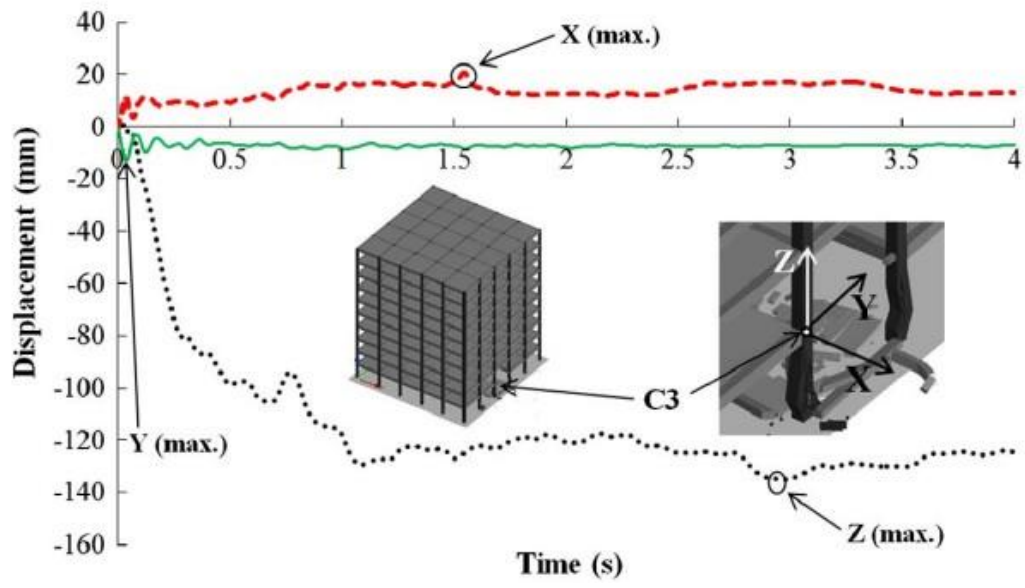
681

682 **Fig. 9.** Response of 4x4 MRF Structures: (a) 3 Stories; (b) 6 Stories; (c) 10 Stories

683

684

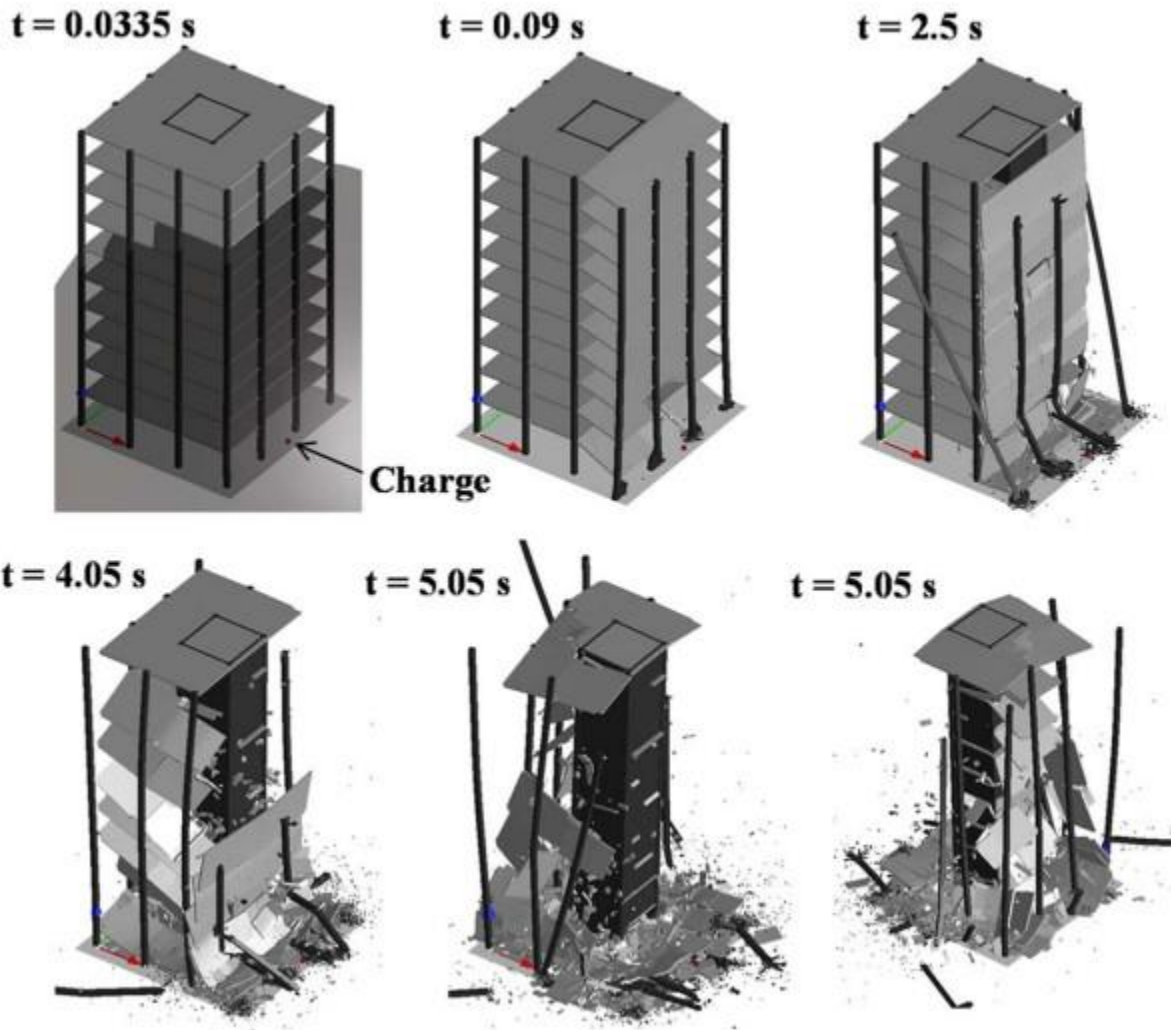
685



686

687 **Fig. 10.** Displacement at Top of Column C3 for the 5x5 MRF Structure

688

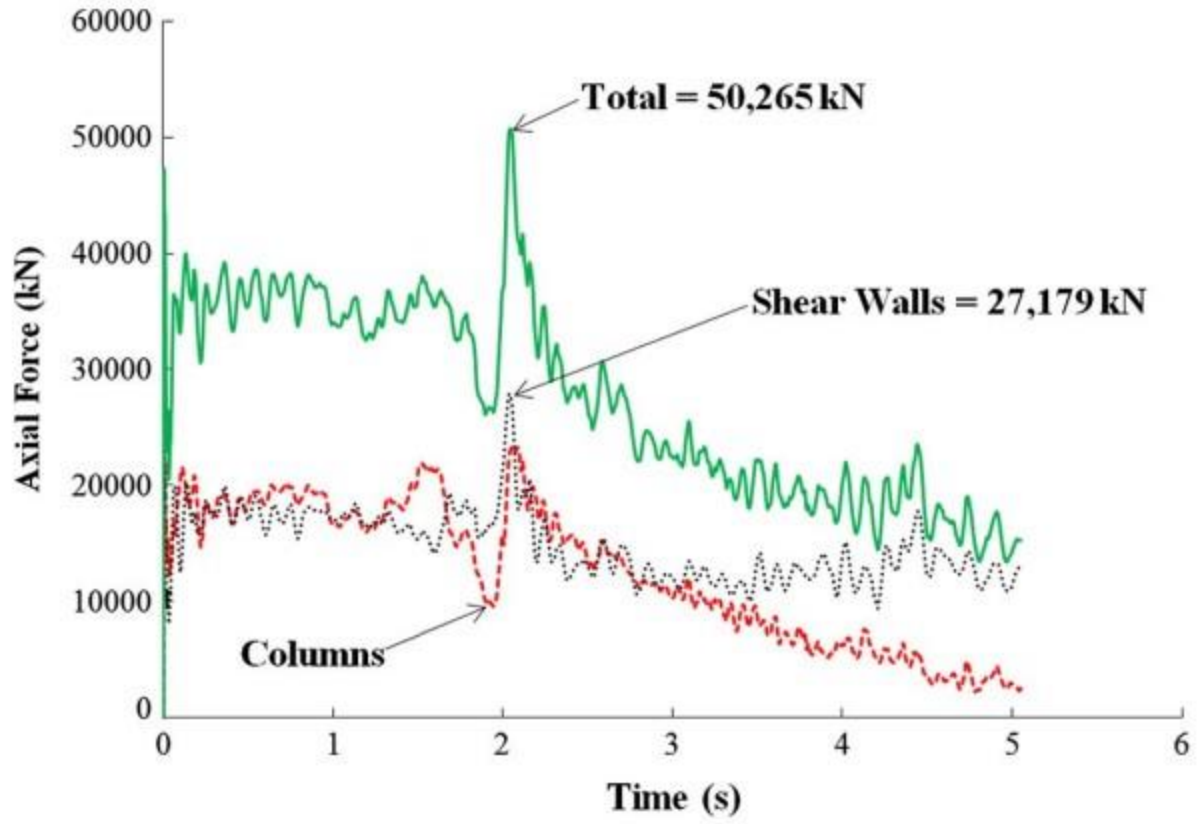


689

690 **Fig. 11.** Response of 3x3 Shear Wall Structure

691

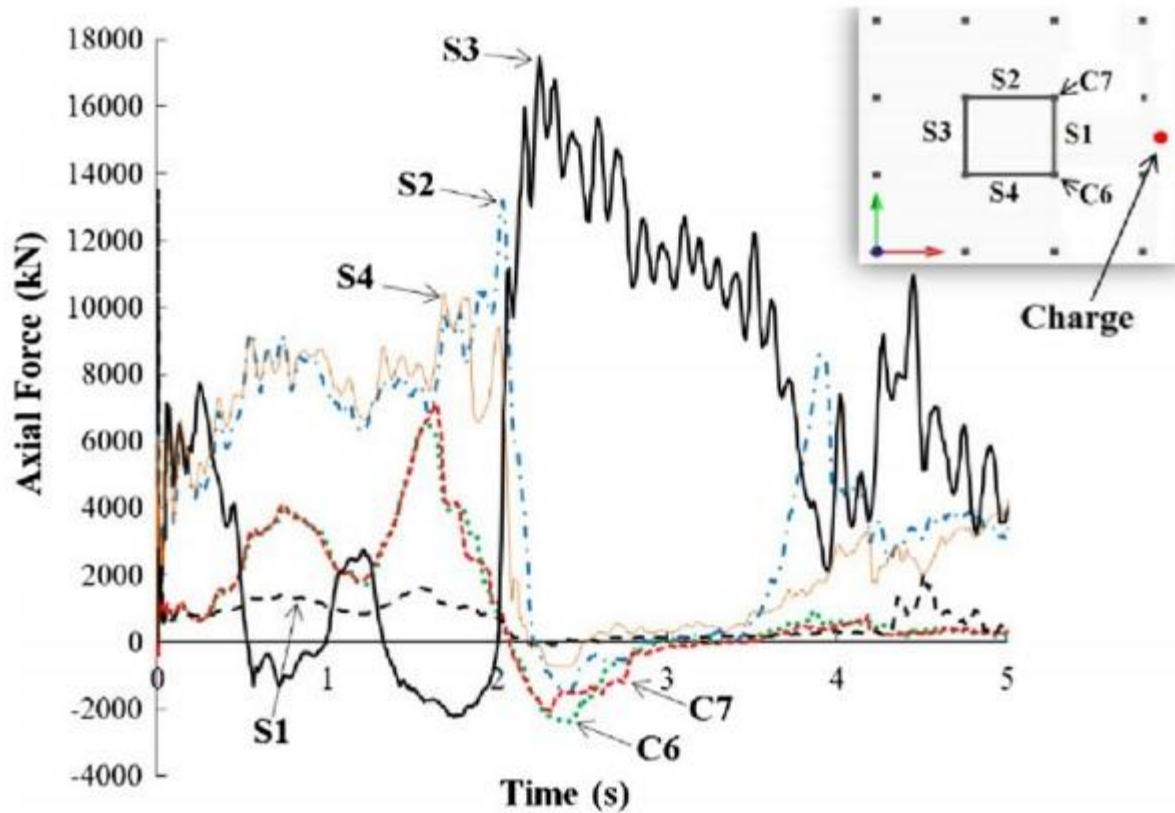
692



693

694 **Fig. 12.** Shear Wall Axial Load Contribution

695

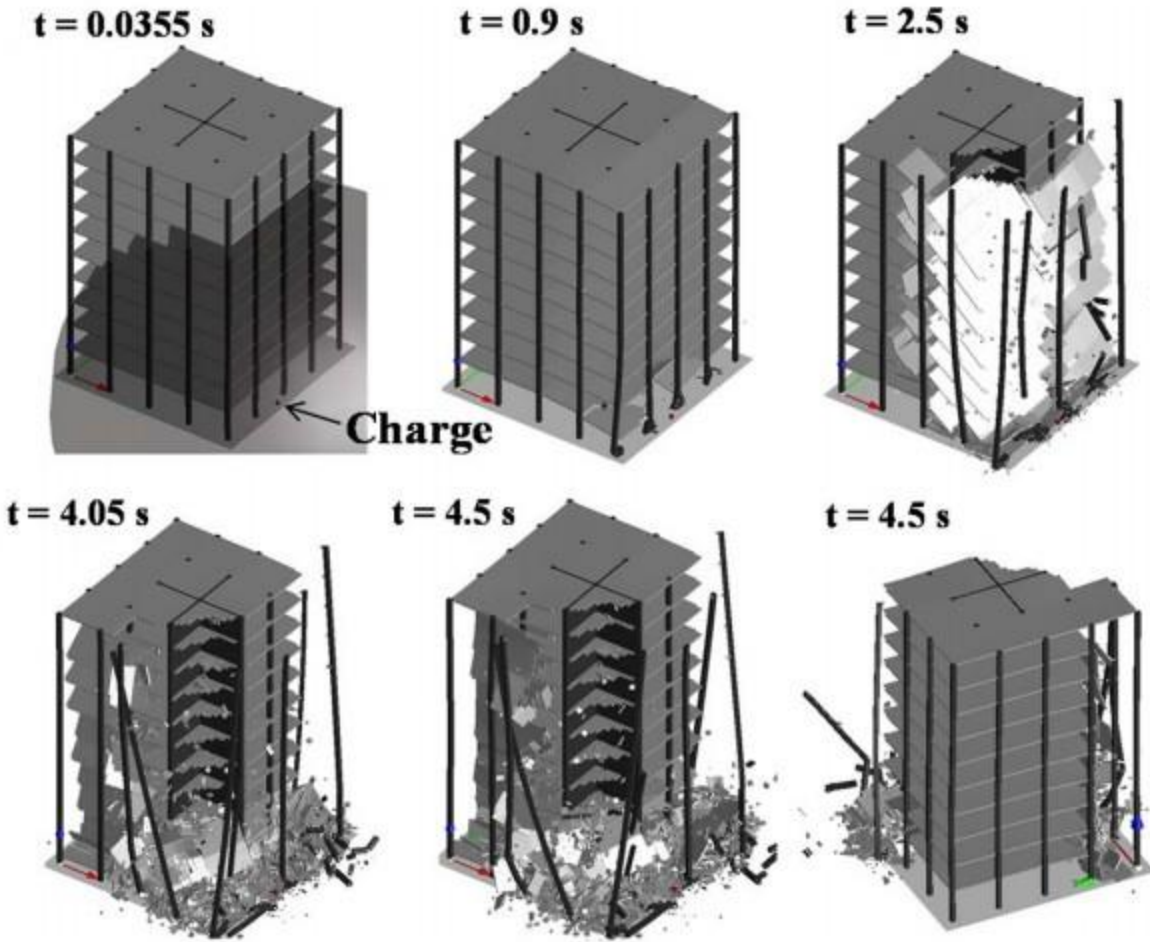


696

697

698 **Fig. 13.** Shear Wall and Column Axial Forces as a Function of Time (3x3 SW)

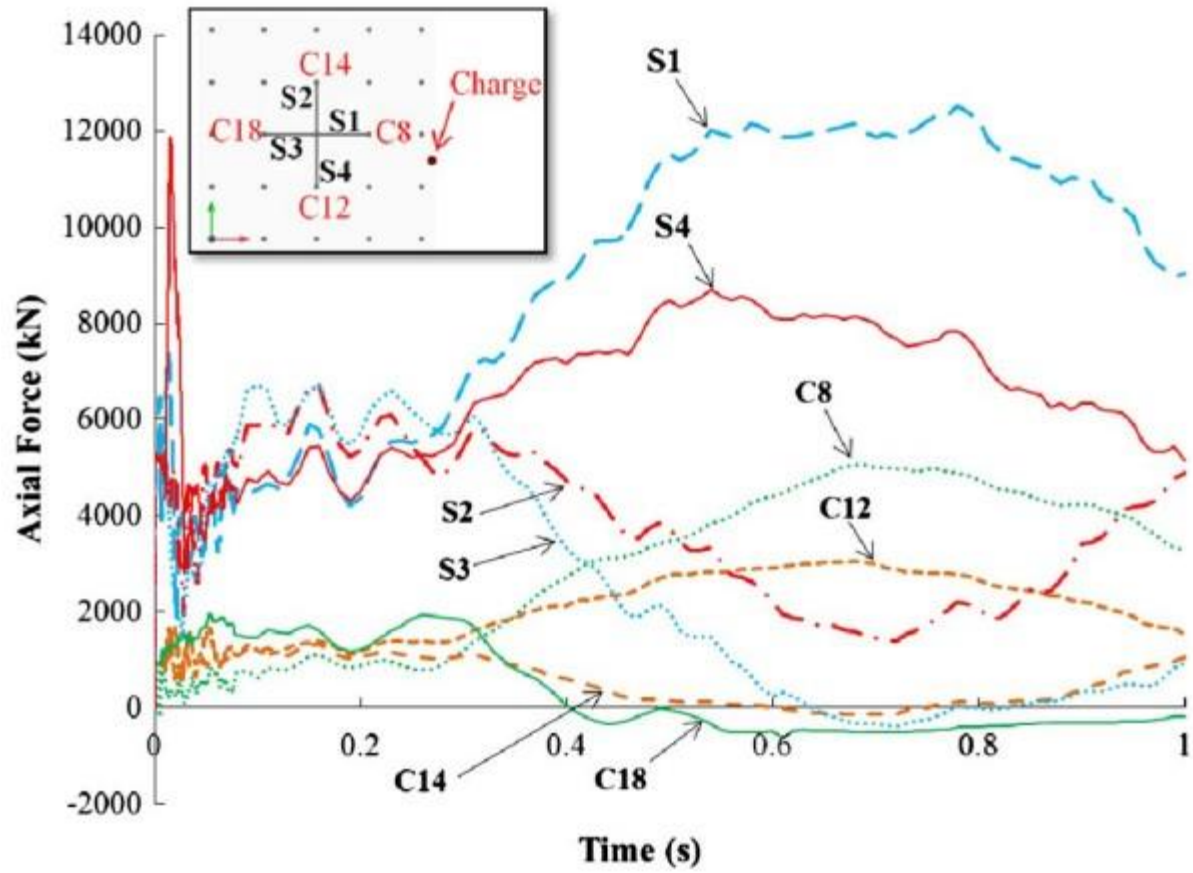
699



700

701 **Fig. 14.** Response of 4x4 Shear Wall Structure

702

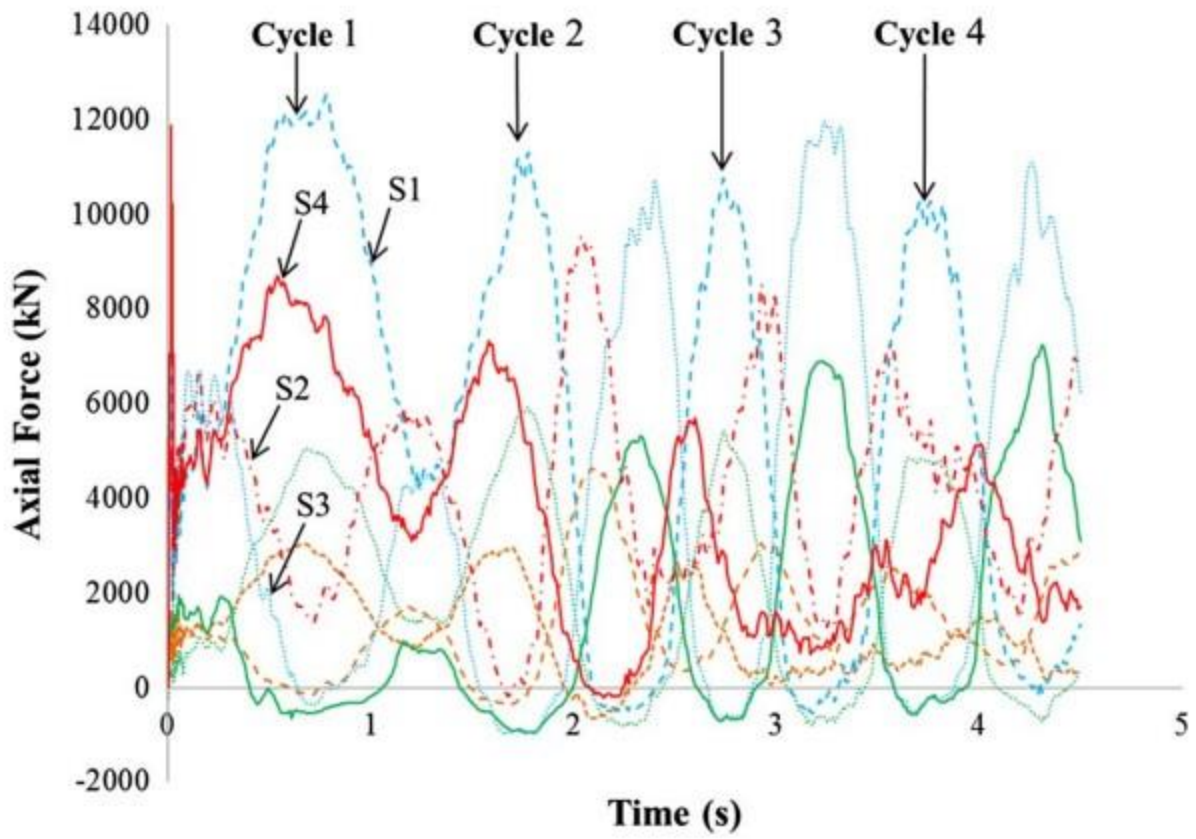


703

704

705 **Fig. 15.** Shear Wall and Column Axial Forces as a Function of Time (4x4 SW)

706

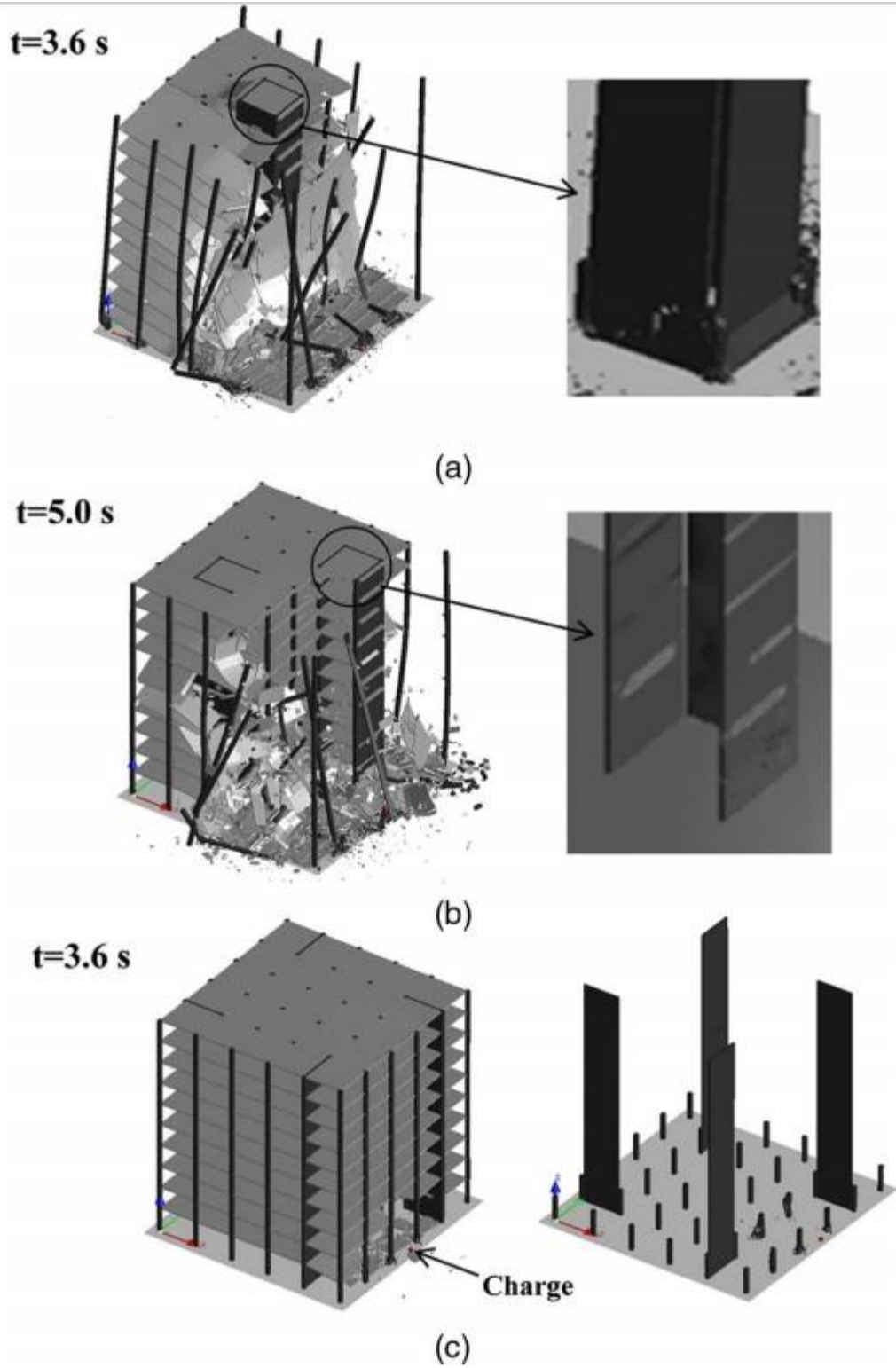


707

708

709 **Fig. 16.** Shear Wall Cyclic Dynamic Response as a Function of Time (4x4 SW)

710



711

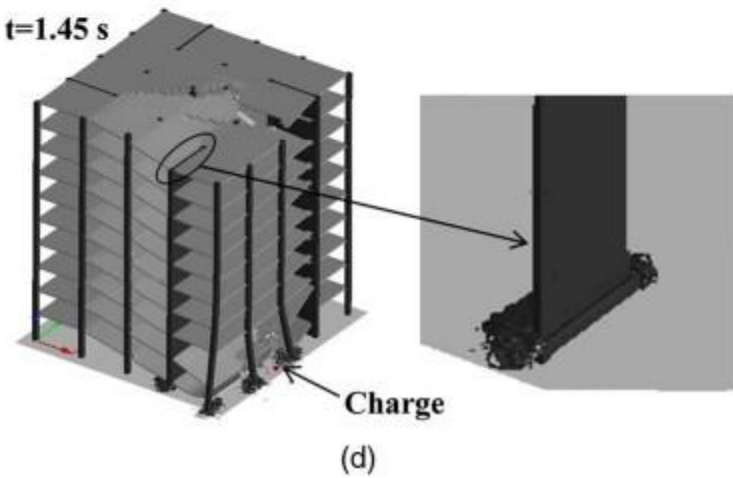
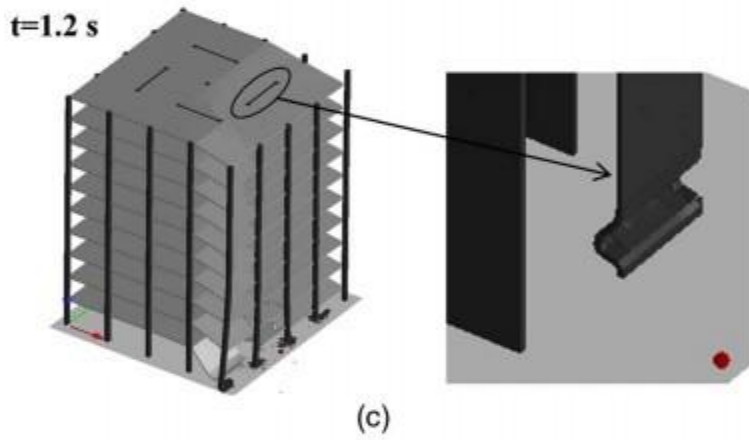
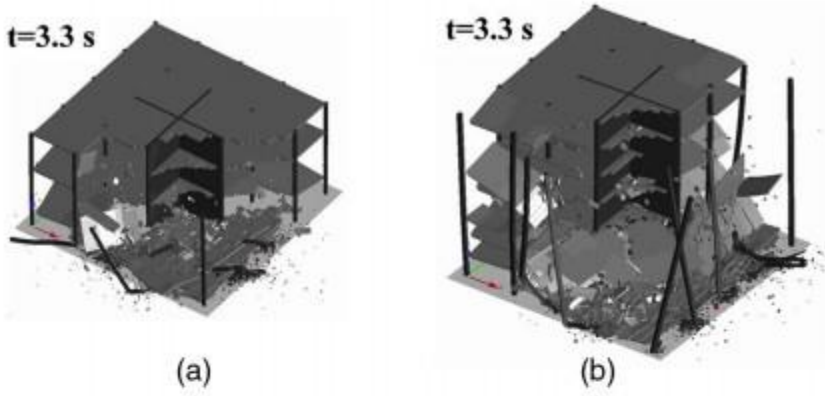
712

713 **Fig. 17.** Response of 4x4 Shear Wall Structure: (a) 3 Stories; (b) 6 Stories; (c & d) 10 Story

714

Alternate Shear Wall Configurations

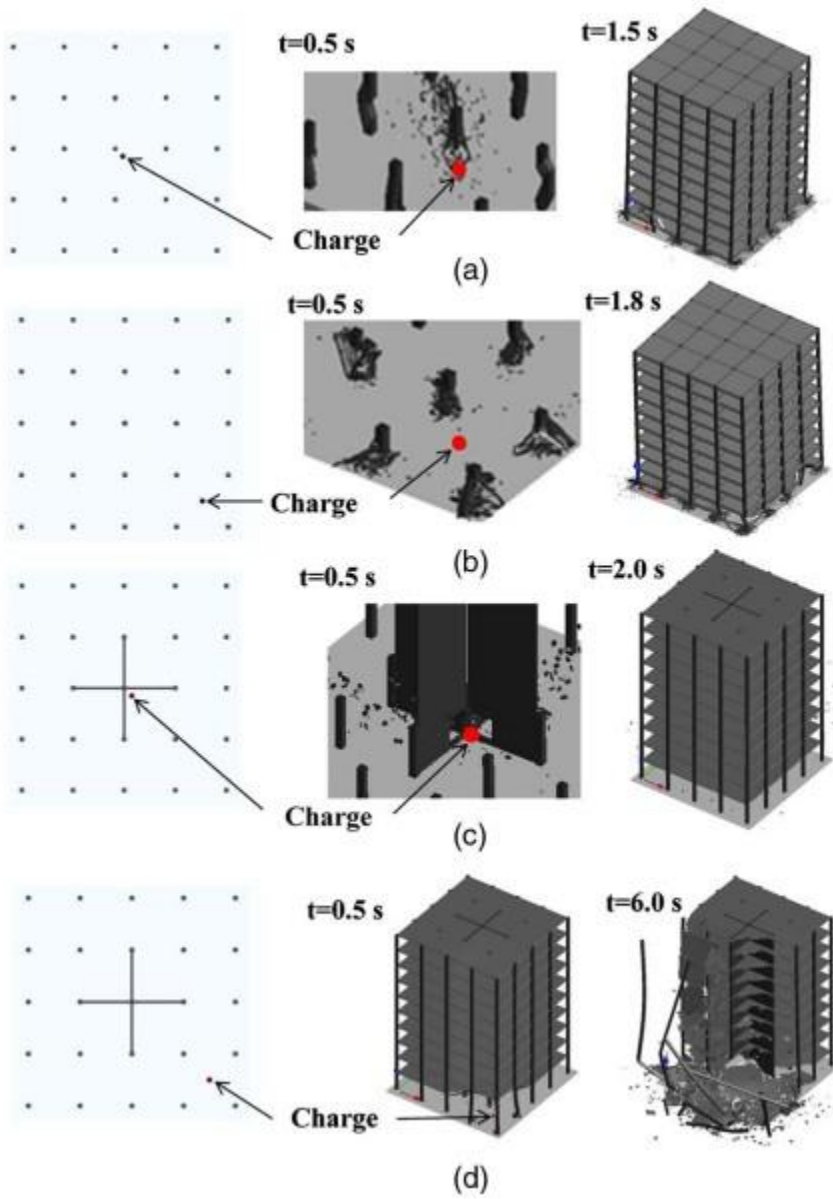
715



716

717

718 **Fig. 18.** Response of 5x5 Shear Wall Structures



720

721

722 **Fig. 19.** Internal Blast Responses of 4x4 MRF and SW Structures

723